

## Emulating Ebbinghaus forgetting behavior in a neuromorphic device based on 1D supramolecular nanofibres

Rao, T.S.; Kundu, S.; Bannur, B.; George, S. J.; Kulkarni, G. U.

**DOI**

[10.1039/D3NR00195D](https://doi.org/10.1039/D3NR00195D)

**Publication date**

2023

**Document Version**

Final published version

**Published in**

Nanoscale

**Citation (APA)**

Rao, T. S., Kundu, S., Bannur, B., George, S. J., & Kulkarni, G. U. (2023). Emulating Ebbinghaus forgetting behavior in a neuromorphic device based on 1D supramolecular nanofibres. *Nanoscale*, 15(16), 7450-7459. <https://doi.org/10.1039/D3NR00195D>

**Important note**

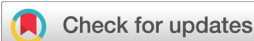
To cite this publication, please use the final published version (if applicable). Please check the document version above.

**Copyright**

Other than for strictly personal use, it is not permitted to download, forward or distribute the text or part of it, without the consent of the author(s) and/or copyright holder(s), unless the work is under an open content license such as Creative Commons.

**Takedown policy**

Please contact us and provide details if you believe this document breaches copyrights. We will remove access to the work immediately and investigate your claim.



Cite this: *Nanoscale*, 2023, **15**, 7450

## Emulating Ebbinghaus forgetting behavior in a neuromorphic device based on 1D supramolecular nanofibres†

Tejaswini S. Rao, ‡<sup>a</sup> Suman Kundu, ‡<sup>b</sup> Bharath Bannur, <sup>a</sup> Subi J. George <sup>c</sup> and Giridhar U. Kulkarni <sup>\*,a</sup>

Mimicking synaptic functions in hardware devices is a crucial step in realizing brain-like computing beyond the von Neumann architecture. 1D nanomaterials with spatial extensions of a few  $\mu\text{m}$ , similar to biological neurons, gain significance given the ease of electrical transport as well as directionality. Herein, we report a two-terminal optically active device based on 1D supramolecular nanofibres consisting of CS (coronene tetracarboxylate) and DMV (dimethyl viologen) forming alternating D–A (donor–acceptor) pairs, emulating synaptic functions such as the STP (short-term potentiation), LTP (long-term potentiation), PPF (paired-pulse facilitation), STDP (spike-time dependent plasticity) and learning–relearning behaviors. In addition, an extensive study on the less explored Ebbinghaus forgetting curve has been carried out. The supramolecular nanofibres being light sensitive, the potential of the device as a visual system is demonstrated using a  $3 \times 3$  pixel array.

Received 12th January 2023,

Accepted 27th March 2023

DOI: 10.1039/d3nr00195d

[rsc.li/nanoscale](https://rsc.li/nanoscale)

## 1 Introduction

Learning and forgetting are important cognitive activities contributing to resource and energy optimization in the human brain. Something not so crucial for life sustenance need not be remembered for long, unlike the present-day practice of reckless storage of bulky data in memory devices! In this direction, researchers have explored the fabrication of devices exhibiting an inherent ability to forget. There are devices that can be optically stimulated to a specific state and, later, electrically erased.<sup>1,2</sup> In some other devices, the erasing is done thermally,<sup>3,4</sup> sometimes only temporarily with the application of force.<sup>5,6</sup> Also, there are systems that have information encoded in them *via* thermal or optical treatments, which self-erase when cooled.<sup>7</sup> In the above examples, although the stored information can be erased selectively, the action is not truly spontaneous and is mostly abrupt. In contrast, the forgetting behavior in living systems is somewhat gradual and

dependent on the incoming information. The real technological progress in this direction would depend on how closely the artificial systems can be made to mimic the bio-counterparts.

The psychological aspect of human learning and forgetting behaviors was put forth for the first time by Hermann Ebbinghaus in 1885.<sup>8</sup> Ebbinghaus showed that learning, if repeated, results in slower forgetting. Also, once the learning is stopped, the forgetting is rapid in the beginning and becomes slower in the latter stages until the information is completely forgotten, and this forgetting nature can be approximated by an exponential function.<sup>9</sup> Although this may seem to follow a familiar trend, its quantitative formulation owes much to the psychologist and hence the name Ebbinghaus forgetting curve. After Ebbinghaus, though several modified mathematical functions have been used in the literature to represent the course of forgetting, it is widely agreed upon by researchers that forgetting retards over time.<sup>10</sup> Thus, the original Ebbinghaus equation still explains the forgetting behavior.

The exponential nature of the forgetting curve is rather straightforward to implement in artificial devices as following the withdrawal of the stimulus, typically an electrical or optical input, the device output tends to decay nearly exponentially due to electrically induced trap states or due to persistent photoconductivity (PPC) arising from filling up of the optically stimulated trap states. The current decay attributed to PPC is similar to the forgetting behavior observed in biological systems, which is well documented.<sup>11</sup> Many artificial synaptic

<sup>a</sup>Chemistry & Physics of Materials Unit, Jawaharlal Nehru Centre for Advanced Scientific Research, Jakkur P. O., Bangalore-560064, India.

E-mail: [kulkarni@jncasr.ac.in](mailto:kulkarni@jncasr.ac.in)

<sup>b</sup>Centre for Nano and Soft Matter Sciences, Shivanasapura, Bangalore-562162, India

<sup>c</sup>Supramolecular Chemistry Laboratory, New Chemistry Unit, Jawaharlal Nehru Centre for Advanced Scientific Research, Bangalore-560064, India

†Electronic supplementary information (ESI) available. See DOI: <https://doi.org/10.1039/d3nr00195d>

‡Tejaswini S. Rao and Suman Kundu contributed equally to this work.

devices exhibiting a current decay behavior analogous to the Ebbinghaus forgetting curve have been reported and are thus being considered potential in the context of cognitive tasks.<sup>12–21</sup> Hu *et al.*<sup>22</sup> have emulated the Ebbinghaus forgetting curve in electrically stimulated NiO-based memristor forming conductive filaments, while Dai *et al.*<sup>23</sup> demonstrated the same in an organic field-effect transistor based on the charge trapping mechanism. Wang *et al.* exploited the PPC effect to mimic the Ebbinghaus learning and forgetting curve in a  $\text{TiN}_x\text{O}_{2-x}/\text{MoS}_2$  heterojunction.<sup>24</sup> Many others report such behavior in devices *via* trap-assisted processes that are mostly optically stimulated.<sup>25–31</sup> It is known that forgetting is also dependent on how information is acquired.<sup>32</sup> The information obtained through prolonged exposure or through rehearsals is well retained, whereas less rehearsed or less exposed information is forgotten faster. The extent of learning, relearning, and rehearsing dictates forgetting. Thus, understanding how the extent of learning affects forgetting behavior poses to be crucial. The present work deals extensively with some of these aspects.

Specifically, we report a simple two-terminal optical neuro-morphic device made with 1D supramolecular nanofibres to emulate various synaptic functions with an emphasis on forgetting behavior. Such device architectures and their functions are rarely reported in the literature (Table S1, ESI†). Supramolecular nanofibres consisting of CS (coronene tetracarboxylate) and DMV (dimethyl viologen) forming alternating D–A (donor–acceptor) pairs and stabilized through charge-transfer interactions are used here as the active material.<sup>33</sup> Being fairly conducting, these fibres have, in the past, served as an active element in humidity sensors,<sup>34</sup> field effect transistors,<sup>35</sup> *etc.* These fibres self-assemble from water, are simple to process without much dependence on lithography, enable miniaturization, reduce carrier scattering, and thereby increase charge transport.<sup>13,36</sup> They undergo self-repair with exposure to humidity,<sup>37</sup> a property that may play an important role in integration. Here, we have exploited the PPC behavior exhibited by the device in emulating the short-term potentiation (STP), long-term potentiation (LTP), the transition from short-term (STM) to long-term memory (LTM), paired-pulse facilitation (PPF), spike-time dependent plasticity (STDP) and learning–forgetting–relearning behaviors. The estimated energy consumption is  $\sim 1.06$  pJ per synaptic junction. A  $3 \times 3$  array has also been prepared to demonstrate the potential of the device architecture as a visual system.

## 2 Experimental

### 2.1 Synthesis of CS–DMV solution

The detailed synthesis procedure of the CS–DMV solution has been reported previously.<sup>33</sup> Briefly, the synthesis of CS (coronene tetracarboxylate) was carried out using a two-fold oxidative benzogenic Diels–Alder reaction of perylene with *N*-ethyl maleimide in the presence of chloranil and *p*-hydroxyanisole followed by hydrolysis with KOH in methanol. The synthesis of

DMV (dodecyl methyl viologen) was carried out using a controlled reaction on one nitrogen of 4,4′-bipyridine with dodecyl bromide to give a monopyridinium ion, followed by its treatment with methyl iodide to give amphiphilic dicationic bipyridine. The charge-transfer fibres were assembled by the injection of a methanol solution of unaggregated DMV into the aqueous solution of free CS molecules (10% v/v methanol in water). The desired concentration of the CS–DMV nanofibre solution was prepared by diluting it with an appropriate amount of deionized water.

### 2.2 Device fabrication

For the fabrication of the supramolecular nanofibre device, a glass substrate was cleaned in piranha solution, followed by washing with acetone, IPA, and distilled water. Interdigitated micro-patterns were developed by photolithography on the glass substrate. Then, microelectrodes were constructed by sputter deposition of Ti followed by a lift-off process. Furthermore, drops (1  $\mu\text{L}$ ) of 0.5 mM CS–DMV supramolecular nanofibre dispersions were drop cast on the interdigitated (IDT) microelectrodes. The devices were vacuum-desiccated overnight to remove excess water.

### 2.3 Characterization

A CHROLIS C1 LED light source (Thorlabs) was used to illuminate the device with the aid of a liquid light guide (LLG) (Thorlabs). The current response of the device was measured using a CH Instruments 660E (Austin, TX, USA) in the two-electrode configuration after making the silver paste contact with the Ti electrodes. The morphology of the nanofibres was examined using a scanning electron microscope (Apreo 2 S SEM, Thermo Fischer Scientific). UV-visible studies were performed using a PerkinElmer Lambda-750 UV-visible spectrophotometer.

## 3 Results and discussion

Fig. 1(a) shows the schematic of the device architecture. The optical microscopy images of the complete device are given in Fig. S1 (ESI†). Details of the fabrication process are given in the Experimental section. The FESEM image of the device (Fig. 1(b)) shows the nanofibres spread across the Ti IDT electrodes. In order to validate the device functioning, IV sweeps were performed, which showed the capacitive nature of the device (Fig. S2, ESI†), in line with an earlier study.<sup>38</sup> The UV-visible absorption spectrum of the supramolecular nanofibres (Fig. S3, ESI†) shows strong absorption peaks at 324 and 357 nm with a broad band centered around 500 nm originating from the ground state charge transfer interaction between the donor and the acceptor molecules.<sup>33</sup> The presence of strong absorption peaks in the UV region prompted us to study the photoresponse behavior of the device; a detailed photodetection study will be carried out separately. In the present study, the performance was monitored using the device current while illuminating it with UV light pulses of 365 nm, as shown in Fig. 1(c). An off-state current of 18 nA was

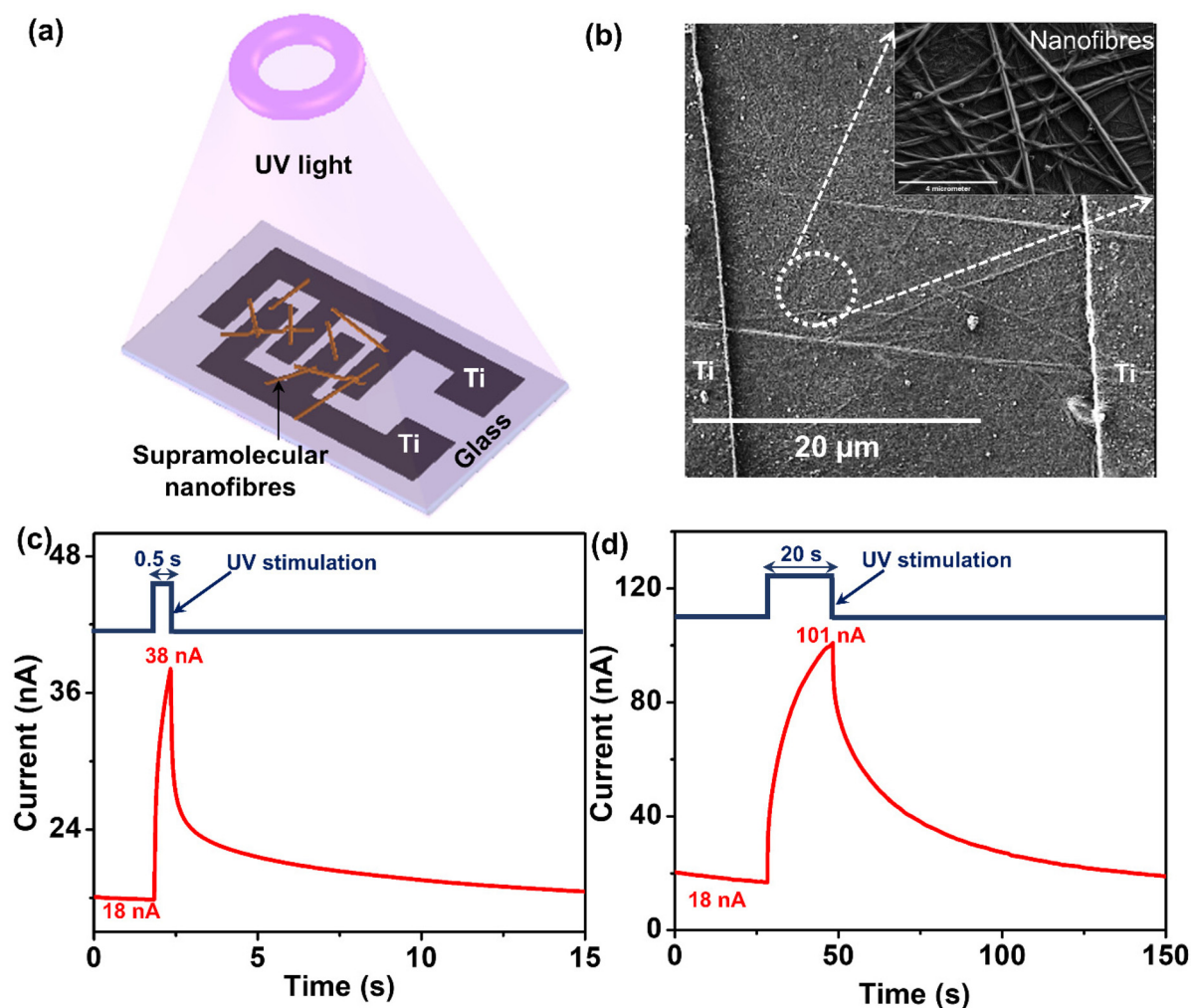


**Fig. 1** (a) Schematic of the supramolecular nanofibre device illuminated with UV light. (b) FESEM image of the device. The inset shows the magnified image of the nanofibre mat spread across the Ti inter-digitated electrodes (Ti IDT). Photoresponse of the device for a single UV light pulse (365 nm,  $6.58 \text{ mW cm}^{-2}$ ) of width (c) 0.5 s and (d) 20 s.

observed for a bias voltage of 1.2 V. On illuminating it with a UV pulse of 0.5 s width, the device current increased to 38 nA, exhibiting the photo-sensing behavior. Interestingly, when the light was turned off, the device current decayed gradually over  $\sim 18$  s to reach its initial value. When the light pulse duration was increased to 20 s (Fig. 1(d)), along with enhancement in the current response to  $\sim 101$  nA, the decay of the current after the light pulse was prolonged ( $\sim 128$  s). This indicates the tunability of the current decay behavior by changing the light pulse parameters. It is known from earlier studies that the conduction in the nanofibre has contributions from both electronic and ionic components, which arise from alternative donor-acceptor charge-transfer pairs with surface hosting ions.<sup>33</sup> The humidity-sensitive nature,<sup>34</sup> p-type behavior,<sup>35</sup> matching of the Fermi level of the nanofibre with the work function of Ti electrodes<sup>38</sup> and delocalization of charge carriers along the  $\pi$ - $\pi$  stacking planes of the donor and acceptor molecules<sup>39</sup> all seem to account for the effective generation and separation of charge carriers upon UV exposure. The

observed decay is attributed to the PPC effect arising due to the trap states that hinder the recombination of the photo-generated charge carriers.<sup>11</sup> This PPC phenomenon exhibited by the device was used to emulate the synapse-like behavior in the nanofibre device. Device functioning as detailed above consumes only  $\sim 1.06$  pJ per synaptic junction (see Note S1, ESI<sup>†</sup>), which is comparable to the reported values from other neuromorphic devices.<sup>40,41</sup>

The biological synapse, pictured as the pivotal unit for achieving complex cognition, is a junction that transmits the received electric impulse from the pre-synaptic neuron to the post-synaptic neuron by releasing neurotransmitters from the synaptic vesicles, thus marking signal transmission. Any changes in the strength of the synaptic connection (also known as the synaptic weight) lead to synaptic plasticity, influencing the temporal profile of the signal transmission. This is the basis of learning, cognition, and memory formation. The biological brain exhibits synaptic functions such as PPF,<sup>42</sup> STP, LTP,<sup>43,44</sup> and STDP<sup>45</sup> responsible for displaying cognitive

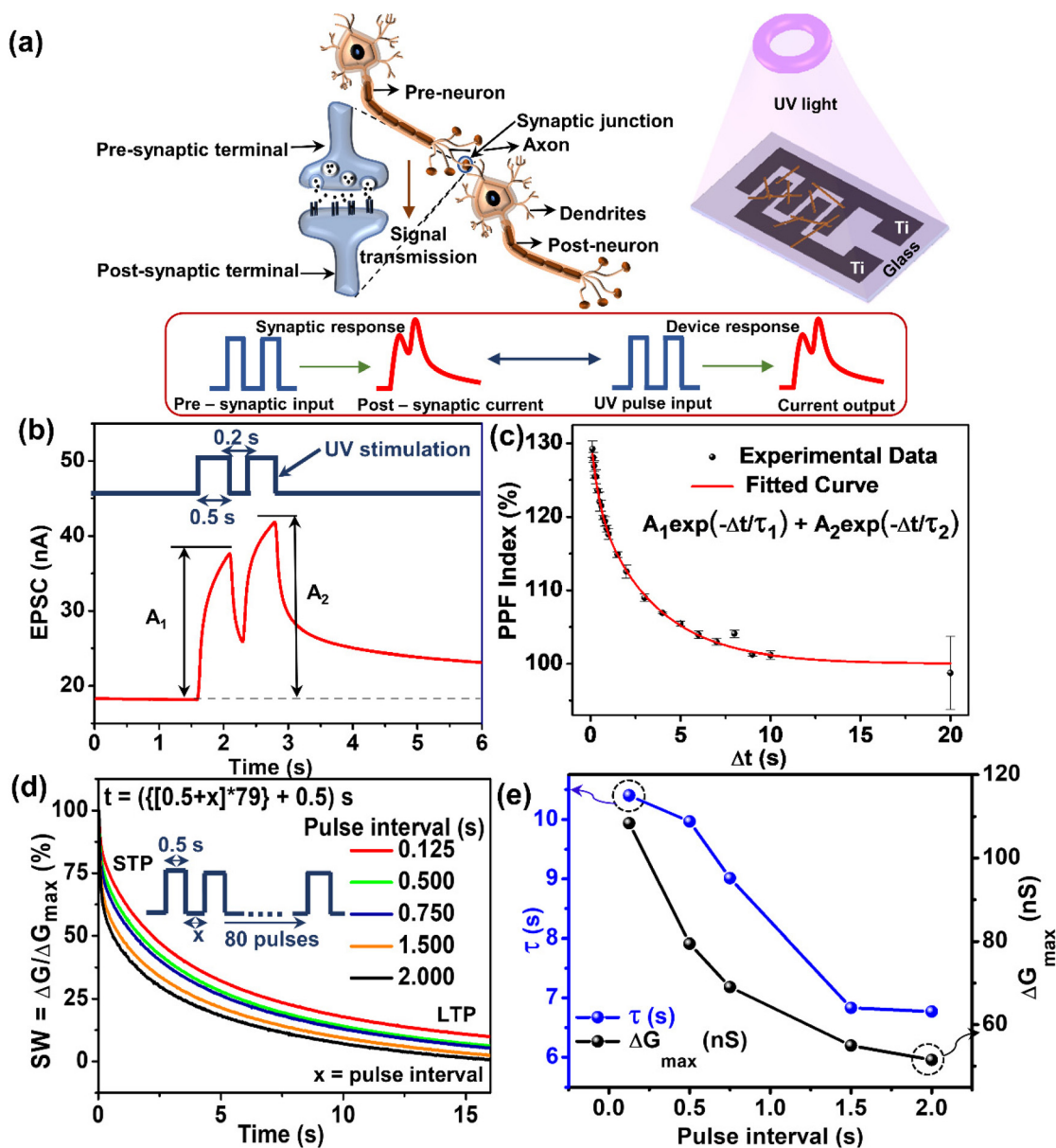


**Fig. 2** (a) Schematic of the biological synapse with an enlarged view (left) depicting the release of neurotransmitters from the synaptic vesicles in the pre-synaptic neuron to the post-synaptic neuron for signal transmission. Schematic of the device exposed to UV pulses (right). The post-synaptic response for the pre-synaptic input, as observed in the biological synapse, is analogous to the current response for the UV pulse input in the device. (b) EPSC of the device for a pair of UV light pulses (width: 0.5 s; interval: 0.2 s). (c) PPF index as a function of UV light pulse interval. (d) Normalized conductance (SW = synaptic weight) against time for varying pulse intervals. (e) Variation of the  $\tau$  and  $\Delta G_{\max}$  with the pulse interval.

activities. Such synaptic functions are emulated in the nanofibre device, as discussed below.

The response of the supramolecular device to the optical stimuli can be thought analogous to the biological synapse, shown in Fig. 2(a). PPF, a form of short-term synaptic plasticity where the response for the second stimulus is enhanced when applied close to the first stimulus, is emulated in the device by applying two UV pulses of 0.5 s width with 0.2 s gap (see Fig. 2(b)). The current response is found to be analogous to the excitatory post-synaptic current (EPSC) that follows the firing of action potential<sup>42</sup> in a biological synapse.

Interestingly, the current in the device for the second UV pulse was greater than that for the first, indicating the facilitation of the second UV pulse by the first UV pulse, leading to the PPF behavior.

The degree of enhancement in the current for the second pulse is given by the PPF index calculated using the equation:

$$\text{PPF index (\%)} = (A_2/A_1) \times 100 \quad (1)$$

where  $A_1$  and  $A_2$  are the current states for the first and the second UV pulses, respectively (Fig. 2(b)).

The PPF index varies with the time interval between the pulses ( $\Delta t$ ) and is shown in Fig. 2(c). The variation can be fitted with the bi-exponential function as shown below:

$$\text{PPF} = C_1 \exp\left(-\frac{\Delta t}{\tau_1}\right) + C_2 \exp\left(-\frac{\Delta t}{\tau_2}\right) \quad (2)$$

The bi-exponential function defines two decay constants,  $\tau_1$  and  $\tau_2$  accounting for the slow and the fast decay behaviors, respectively. The PPF index, thus, explains that the information coding is effective with a shorter pulse interval and lessens with longer intervals.  $C_1$  and  $C_2$  are the facilitation magnitudes for the slow and the fast decay behaviors, respectively.<sup>46</sup>

From Fig. 2(c), it is observed that a smaller pulse interval results in greater facilitation, while a larger pulse interval leads to poor facilitation. The values of  $C_1 = 23$ ,  $C_2 = 8$ ,  $\tau_1 = 3390$  s and  $\tau_2 = 429$  s are obtained by fitting the experimentally obtained results with eqn (2). The slow decay is facilitated more than the fast decay, as given by  $C_1$  and  $C_2$ , respectively. However, the slow decay takes a longer time than the fast decay, as observed from the values of  $\tau_1$  and  $\tau_2$ , respectively. The facilitation was then extended to a larger number (80) of pulses of 0.5 s width while varying the pulse intervals (0.125 to 2 s) for each set. The device showed an increase in the current response for subsequent pulses, prominently visible when the pulse interval was smaller (Fig. S4, ESI<sup>†</sup>). Also, the current decay was slower for the 0.125 s pulse interval than at larger time intervals (Fig. 2(d)). It is evident that the device exhibits memory formation and retention akin to the biological systems – a repeated in-flow of information at smaller time gaps results in a stronger acquisition with longer retention (slower forgetting). The initial faster decay followed by a slower decay of the current in the device is analogous to the STP and LTP components of the biological synapse. The more prominent STP component results in short-term memory, and a significant LTP component shows a transition from short-term memory (STM) to long-term memory (LTM).<sup>10,47</sup> Accordingly, the current decay for the 2 s interval produces a prominent STP component, whereas the 0.125 s interval shows a significant LTP, exhibiting the STM to LTM transition (Fig. 2(e)), similar to the forgetting behavior in humans.

The Ebbinghaus forgetting curve<sup>22</sup> is most widely used in the literature as it rightly explains the forgetting behavior and is also supported by many psychological experiments. Indeed, many forgetting functions reported in the literature have also been tried out (Fig. S5(a)–(f), ESI<sup>†</sup>);<sup>9,48</sup> however, the Ebbinghaus forgetting function fitted the best for the nanofibre device as well. Other equations (e.g., the sum of exponentials, double and triple) fail to account for the forgetting behavior satisfactorily,<sup>9</sup> whereas logarithmic and power functions behave poorly under the boundary conditions and are shown to produce poorer fits in some psychological experiments. Besides, the Ebbinghaus forgetting curve is advantageous as it explains the decay taking place at different time scales (fast and slow processes). Specifically, in the simplest form, the

parameter  $\beta$  explains the degree of deviation from an exponential function.

$$\frac{\Delta G}{\Delta G_{\max}} = \exp\left(-\left(\frac{t}{\tau}\right)^\beta\right) \quad (3)$$

Here,  $\Delta G/\Delta G_{\max}$  is the synaptic weight change.  $\Delta G = (G - G_0)$  is the difference between the conductance at time 't' and the initial dark state conductance,  $\Delta G_{\max} (=G_{\max} - G_0)$  is the difference between the peak conductance and the initial dark state conductance,  $\tau$  is the relaxation time constant, and  $\beta$  is the stretching exponent. The decreasing  $\tau$  and  $\Delta G_{\max}$  values (Fig. 2(e)) with an increasing pulse interval further confirms the STM to LTM transition.

The observation of information for a longer time results in stronger learning and slower forgetting. The same is emulated here by varying the UV exposure time (Fig. S6(a), ESI<sup>†</sup>). With longer UV exposure time, the device forgets the learned information slowly, as reflected in the STP and the LTP components (Fig. 3(a)). The slower forgetting with the UV exposure time additionally indicates the transfer of information from STM to LTM. The increments in  $\tau$  (obtained from the Ebbinghaus forgetting equation, see Fig. 3(b)) and  $\Delta G_{\max}$  with different UV exposure time periods stand for slower forgetting and greater memory retention, respectively. Greater retention also occurs when a piece of information is learned frequently. With an increase in the UV pulse frequency (Fig. S6(b), ESI<sup>†</sup>), the decay becomes slower, resulting in the STM to LTM transition, as shown in Fig. 3(c). Both  $\tau$  and  $\Delta G_{\max}$  increase with frequency, accounting for the alteration in the memory strength for varying frequencies (Fig. 3(d)). Besides, a piece of information is learned faster and stays longer when it is presented with a higher intensity. The device shows a higher response for an increase in intensity (Fig. S6(c), ESI<sup>†</sup>) and retains the obtained response longer, as shown in Fig. 3(e). In addition, the increments in  $\tau$  and  $\Delta G_{\max}$  with intensity mimic the STM to LTM transition (Fig. 3(f)). Instead of fixed (80) pulses, experiments were performed by varying the number of pulses as well (see Fig. 4(a) and Fig. S7, ESI<sup>†</sup>), and the STM to LTM transition was again evident. Both values,  $\tau$  and  $\Delta G_{\max}$ , increased with the number of pulses (Fig. 4(b)), corresponding to a slower forgetting. Another experiment involved two sets of pulses with a sufficient gap between the two, such that the second set was applied slightly before the previous current decayed (Fig. 4(c)). Interestingly, less number of pulses (25) were required in the second set to reach a current value that otherwise would take a larger first set (35). Thus, the rate of relearning is 16% faster than the learning process. The learning, forgetting, and relearning behavior observed here is akin to humans.

Another important synaptic activity is STDP, where the temporal correlation between the pre- and post-synaptic activities governs the strength of learning and describes long-term synaptic plasticity (LTP/LTD – long-term potentiation/depression).<sup>49,50</sup> The connection strength between the synapses varies with the time interval ( $\Delta t$ ) of the pre- and the post-spikes. Among the two forms of STDP, symmetric and asymmetric, representing the Hebbian law, symmetric STDP is known to play a crucial role in

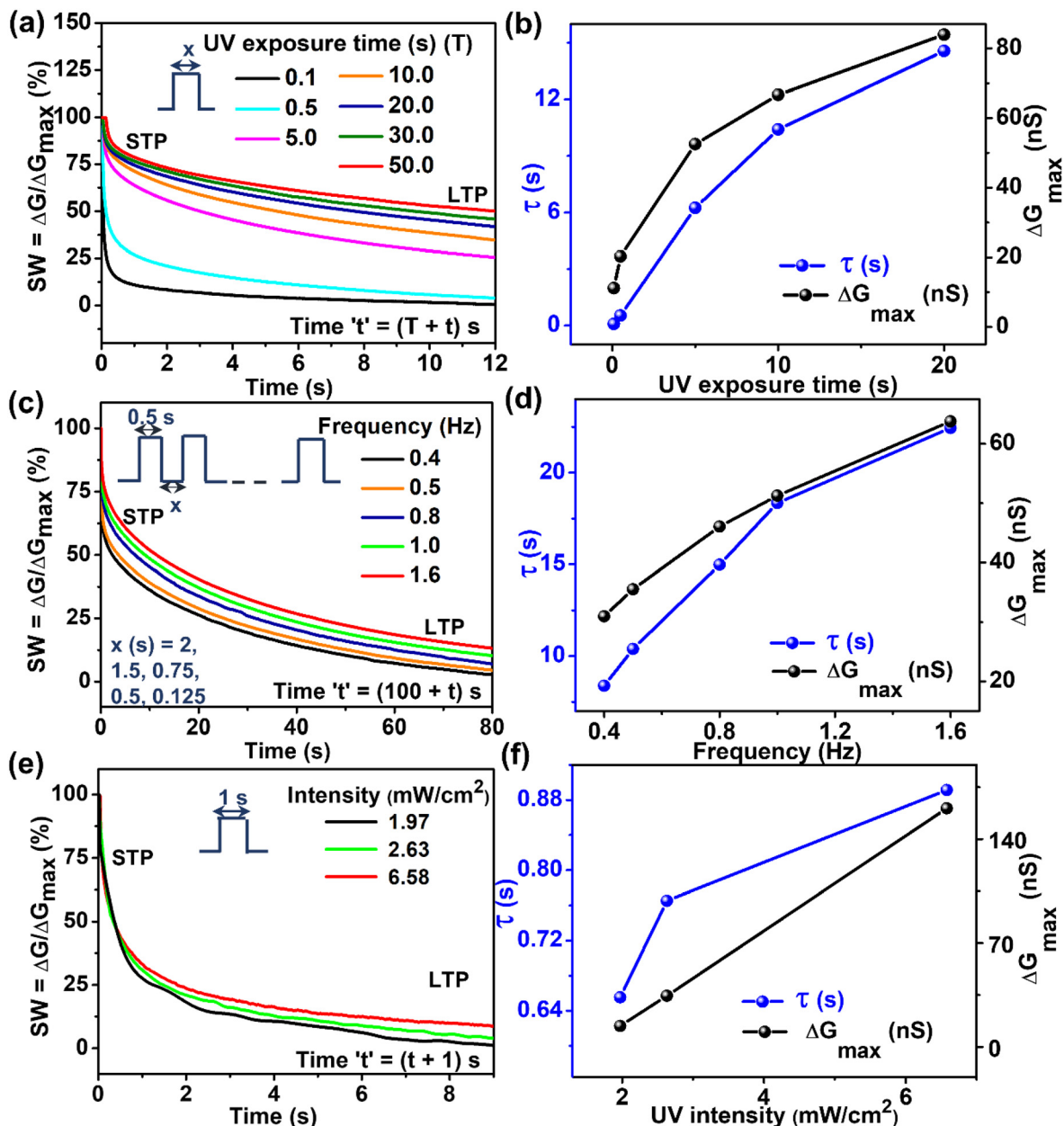


**Fig. 3** (a) Normalized conductance against time for different UV exposure times. (b) Variation of  $\tau$  and  $\Delta G_{max}$  with the UV exposure time. (c) Normalized conductance against time for different frequencies. (d) Variation of  $\tau$  and  $\Delta G_{max}$  with the frequency. (e) Normalized conductance against time for varying intensities. (f) Variation of  $\tau$  and  $\Delta G_{max}$  with the intensity.

auto-associative models.<sup>51,52</sup> Symmetric STDP was emulated by connecting two devices (one was considered as a pre-synapse and the other post-synapse) and exposing each device to UV pulses at different time intervals,  $\Delta t$ , as shown in the schematic (Fig. 5(a)). The current response from each device was recorded on UV exposure, and the change in conductance was calculated as:

$$\Delta G = (G_2 - G_1) / G_1 \quad (\%) \quad (4)$$

for each  $\Delta t$ . The  $\Delta t$  value was varied from  $-1.0$  to  $+1.0$  s. The STDP characteristics were derived by plotting  $\Delta G$  as a function

of  $\Delta t$ , as shown in Fig. 5(b). The conductance change increases with smaller  $\Delta t$  and decreases, both positively and negatively, as  $\Delta t$  becomes larger. This indicates that the synaptic connection strengthens with a smaller  $\Delta t$  and weakens as the  $\Delta t$  increases, thus emulating STDP.

Furthermore, the learning and forgetting behavior of the device was emulated using a  $3 \times 3$  visual pixel array (see Fig. 6(a)). There are such reports on the emulation of advanced cognitive behaviors<sup>53-55</sup> and artificial visual perception<sup>56,57</sup> using optoelectronic devices. In the present device, five 'T' shaped pixels were exposed to UV light under similar con-

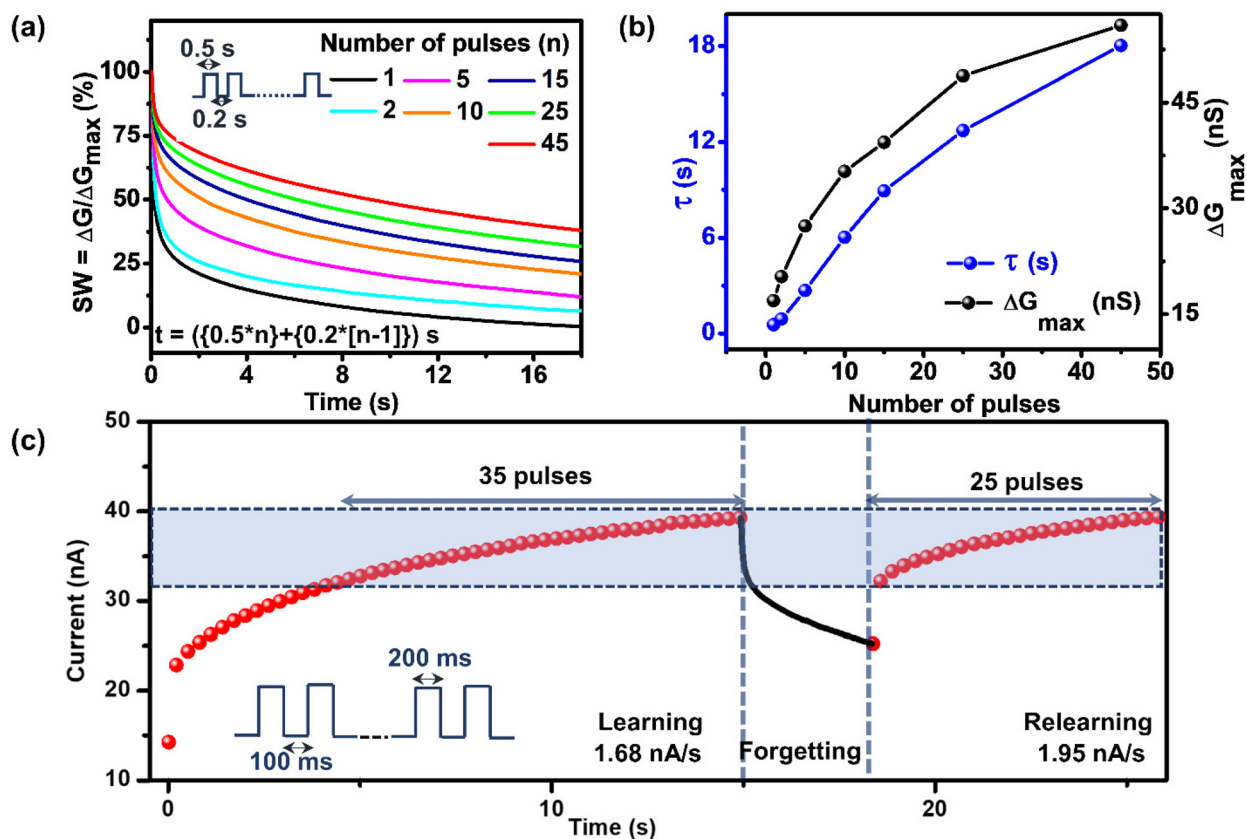


Fig. 4 (a) Normalized conductance against time for varying number of pulses (width: 0.5 s, interval: 0.2 s). (b) Variation of  $\tau$  and  $\Delta G_{\max}$  with the number of pulses. (c) Emulation of the learning–forgetting–relearning behavior.

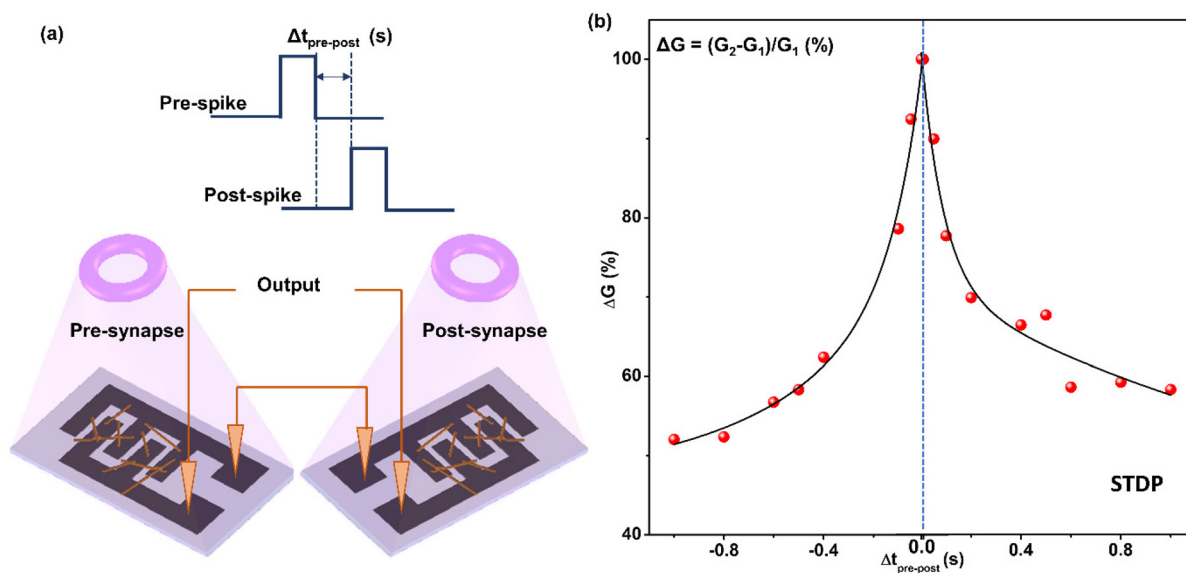
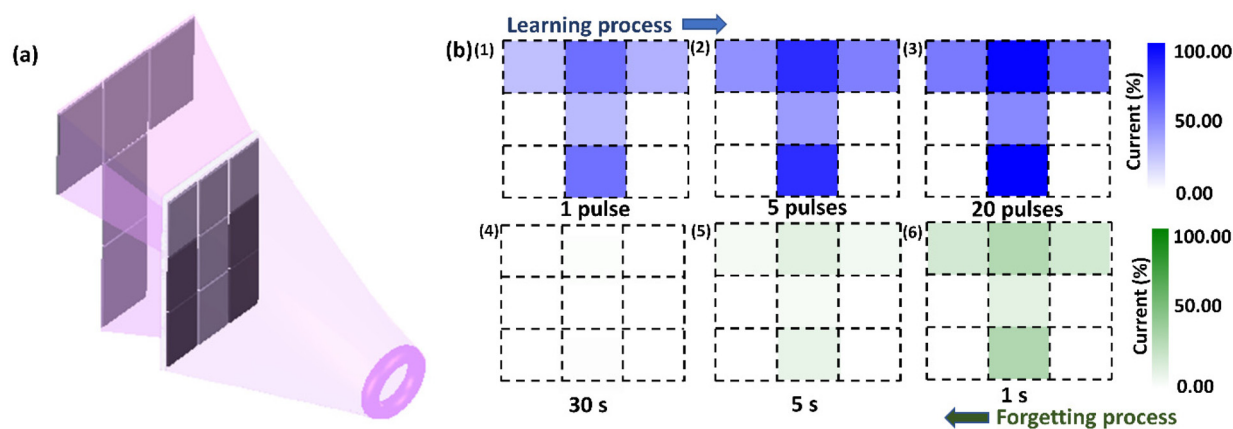


Fig. 5 (a) Schematic of two devices used for the emulation of spike-time dependent plasticity (bottom panel). The top panel shows the input pre- and post-spike, applied to the pre- and post-synaptic devices, respectively, with the time interval,  $\Delta t$ . (b) Variation in the connection strength as a function of  $\Delta t$ , exhibiting symmetric STDP.



**Fig. 6** (a) Schematic of the  $3 \times 3$ -pixel array. (b) The  $3 \times 3$ -pixel arrays emulate the learning and forgetting process. In the learning process, the current in response to a given number of UV pulses (up to 20 pulses, 1–3) represents the strength of learning as indicated by the color code. With no further illumination, the forgetting process sets in with current values (shown by the green color code, 4–6) in different pixels diminishing with time.

ditions, while the remaining four were masked. The current response with an increase in the number of UV light pulses (Fig. S8, ESI†) represents varying strengths in learning. When the current response was color mapped, the alphabet ‘T’ which was prominently formed after a UV exposure, became dull with time; after 30 s, the symbol was nearly completely forgotten (Fig. 6(b)). The learning and forgetting processes exhibited are similar to those in the human brain, further demonstrating the potential of the device to mimic the synaptic functionalities.

## 4 Conclusions

A neuromorphic two-terminal device with 1D supramolecular nanofibres as the photoactive element has been prepared. The inherent PPC effect of the device for UV light was exploited to mimic various synaptic functions such as the STP, LTP, PPF, STDP, and learning–relearning behaviors by varying the UV pulse parameters. With decreasing time intervals, from 20 to 0.1 s, PPF was realized. Similarly, the STP–LTP behavior was emulated by applying 80 pulses of varied time intervals (from 0.125 to 2 s), by varying the UV exposure time (from 0.1 to 50 s), frequency (from 0.4 to 1.6 Hz), intensity (from 1.97 to 6.58  $\text{mW cm}^{-2}$ ) and the number of pulses (from 1 to 45). Overall, the current decay exhibited by the device after the UV light termination was found to resemble the forgetting behavior in humans, typified by the Ebbinghaus forgetting equation. The learning–relearning behavior in 1D fibres was further examined by applying the second set of pulses before the complete decay of the first set. The relearning needed a less number of pulses, signifying that relearning is faster than learning. A symmetric STDP was produced by varying the time interval  $\Delta t$  from  $-1$  to  $+1$  s, where the synaptic connection strength increased with smaller  $\Delta t$  and decreased with larger  $\Delta t$ , on both positive and negative scales. A  $3 \times 3$  pixel array responding to controlled exposure to UV light has been

demonstrated, establishing the potential of the device as a visual system. The incorporation of a simple device architecture with the utilization of 1D organic nanofibres to mimic the various synaptic functions is a step forward in achieving parallel processing, in turn, brain-like computing.

## Author contributions

Tejaswini S. Rao and Suman Kundu contributed equally. The manuscript was written through the contributions of all authors. All authors have approved the final version of the manuscript.

## Conflicts of interest

There are no conflicts to declare.

## Acknowledgements

The authors acknowledge the Department of Science and Technology (DST), India, for the funding. The authors thank JNCASR for the facilities. Tejaswini S. Rao acknowledges the INSPIRE fellowship from DST, India.

## References

- 1 D. Zheng, J. Zhang, X. He, Y. Wen, P. Li, Y. Wang, Y. Ma, H. Bai, H. N. Alshareef and X. X. Zhang, *Nanoscale*, 2022, **14**, 12339.
- 2 B. Liu, J. Liu, L. Lv, Y. Hou, J. Shen and B. Zhang, *ACS Appl. Electron. Mater.*, 2021, **3**, 1006.
- 3 Y. Liu, Y. Yang, D. Shi, M. Xiao, L. Jiang, J. Tian, G. Zhang, Z. Liu, X. Zhang and D. Zhang, *Adv. Mater.*, 2019, **31**, 1902576.

- 4 S. Khlifi, N. Fournier Le Ray, S. Paofai, M. Amela-Cortes, H. Akdas-Kiliç, G. Taupier, S. Derien, S. Cordier, M. Achard and Y. Molard, *Mater. Today*, 2020, **35**, 34.
- 5 H. Xuan, Q. Guan, H. Tan, H. Zuo, L. Sun, Y. Guo, L. Zhang, R. E. Neisiany and Z. You, *ACS Nano*, 2022, **16**, 16954.
- 6 L. Jiang, J. Li, N. Peng, M. Gao, D.-Y. Fu, S. Zhao and G. Li, *Polymer*, 2022, **263**, 125509.
- 7 Z. Fang, X. Lin, Y. Lin, J. Gao, L. Gong, R. Lin, G. Pan, J. Wu, W. Lin, X. Chen and G. Yi, *Nano Res.*, 2022, **10**, 634.
- 8 H. Ebbinghaus, *Translation of Memory: A Contribution to Experimental Psychology*, Columbia University, New York, 1913.
- 9 J. M. J. Murre and J. Dros, *PLoS One*, 2015, **10**, e0120644.
- 10 J. T. Wixted and E. B. Ebbesen, *Psychol. Sci.*, 1991, **2**, 409.
- 11 A. Sumanth, K. Lakshmi Ganapathi, M. S. Ramachandra Rao and T. Dixit, *J. Phys. D: Appl. Phys.*, 2022, **55**, 393001.
- 12 Y. Abbas, A. S. Sokolov, Y. R. Jeon, S. Kim, B. Ku and C. Choi, *J. Alloys Compd.*, 2018, **759**, 44.
- 13 Y. S. Zhao, H. Fu, A. Peng, Y. Ma, Q. Liao and J. Yao, *Acc. Chem. Res.*, 2010, **43**, 409.
- 14 J. Gong, H. Yu, X. Zhou, H. Wei, M. Ma, H. Han, S. Zhang, Y. Ni, Y. Li and W. Xu, *Adv. Funct. Mater.*, 2020, **30**, 2005413.
- 15 T. Kim, J. W. Lim, S. J. Yun, S. H. Lee and K. H. Jung, *Adv. Electron. Mater.*, 2020, **6**, 1901044.
- 16 L. Li, Y. Shao, X. Wang, X. Wu, W. J. Liu, D. W. Zhang and S. J. Ding, *IEEE Trans. Electron Devices*, 2020, **67**, 105.
- 17 X. Liang, X. Chen, X. Yang and J. Ni, *Nanotechnology*, 2021, **32**, 025706.
- 18 A. S. Sokolov, H. Abbas, Y. Abbas and C. Choi, *J. Semicond.*, 2021, **42**, 013101.
- 19 N. Ilyas, D. Li, C. Li, X. Jiang, Y. Jiang and W. Li, *Nanoscale Res. Lett.*, 2020, **15**, 30.
- 20 Y. Wang, F. Wang, Z. Wang, J. Wang, J. Yang, Y. Yao, N. Li, M. G. Sendeku, X. Zhan, C. Shan and J. He, *Nano Res.*, 2021, **14**, 4328.
- 21 M. Wu, S. Shang, Q. Wei, C. Liu, A. Li, X. Gao, S. Wang, J. Yin, Y. Xia and Z. Liu, *Adv. Electron. Mater.*, 2020, **6**, 1901255.
- 22 S. G. Hu, Y. Liu, T. P. Chen, Z. Liu, Q. Yu, L. J. Deng, Y. Yin and S. Hosaka, *Appl. Phys. Lett.*, 2013, **103**, 133701.
- 23 S. Dai, X. Wu, D. Liu, Y. Chu, K. Wang, B. Yang and J. Huang, *ACS Appl. Mater. Interfaces*, 2018, **10**, 21472.
- 24 W. Wang, S. Gao, Y. Li, W. Yue, H. Kan, C. Zhang, Z. Lou, L. Wang and G. Shen, *Adv. Funct. Mater.*, 2021, **31**, 2101201.
- 25 H. Bian, X. Qin, Y. Wu, Z. Yi, S. Liu, Y. Wang, C. D. S. Brites, L. D. Carlos and X. Liu, *Adv. Mater.*, 2021, **34**, 2101895.
- 26 E. Ercan, Y. Lin, W. Yang and W. Chen, *Adv. Funct. Mater.*, 2022, **32**, 2107925.
- 27 X. Wang, X. Zhou, A. Cui, M. Deng, X. Xu, L. Xu, Y. Ye, K. Jiang, L. Shang, L. Zhu, J. Zhang, Y. Li, Z. Hu and J. Chu, *Mater. Horiz.*, 2021, **8**, 1985.
- 28 J. Y. Chen, D. L. Yang, F. C. Jhuang, Y. H. Fang, J. S. Benas, F. C. Liang and C. C. Kuo, *Adv. Funct. Mater.*, 2021, **31**, 2105911.
- 29 T. Ahmed, S. Kuriakose, E. L. H. Mayes, R. Ramanathan, V. Bansal, M. Bhaskaran, S. Sriram and S. Walia, *Small*, 2019, **15**, 1900966.
- 30 T. R. Lin, L. C. Shih, P. J. Cheng, K. T. Chen and J. S. Chen, *RSC Adv.*, 2020, **10**, 42682.
- 31 S. Lan, J. Zhong, J. Chen, W. He, L. He, R. Yu, G. Chen and H. Chen, *J. Mater. Chem. C*, 2021, **9**, 3412.
- 32 R. C. Atkinson and R. M. Shiffrin, Human Memory: A Proposed System and its Control Processes, in *Psychology of Learning and Motivation*, ed. K. W. Spence and J. T. Spence, Elsevier, London, 1968, vol. 2, p. 89.
- 33 K. V. Rao, K. Jayaramulu, T. K. Maji and S. J. George, *Angew. Chem.*, 2010, **122**, 4314.
- 34 U. Mogera, A. A. Sagade, S. J. George and G. U. Kulkarni, *Sci. Rep.*, 2014, **4**, 4103.
- 35 A. A. Sagade, K. V. Rao, U. Mogera, S. J. George, A. Datta and G. U. Kulkarni, *Adv. Mater.*, 2013, **25**, 559.
- 36 D. Panda and T. Y. Tseng, *J. Mater. Sci.*, 2013, **48**, 6849.
- 37 U. Mogera, M. Gedda, S. J. George and G. U. Kulkarni, *ACS Appl. Mater. Interfaces*, 2017, **9**, 32065.
- 38 S. Kundu, U. Mogera, S. J. George and G. U. Kulkarni, *Nano Energy*, 2019, **61**, 259.
- 39 N. Wu, C. Wang, P. M. Slattum, Y. Zhang, X. Yang and L. Zang, *ACS Energy Lett.*, 2016, **1**, 906.
- 40 T. Wang, J. Meng, X. Zhou, Y. Liu, Z. He, Q. Han, Q. Li, J. Yu, Z. Li, Y. Liu, H. Zhu, Q. Sun, D. W. Zhang, P. Chen, H. Peng and L. Chen, *Nat. Commun.*, 2022, **13**, 7432.
- 41 C. Yang, J. Qian, S. Jiang, H. Wang, Q. Wang, Q. Wan, P. K. L. Chan, Y. Shi and Y. Li, *Adv. Opt. Mater.*, 2020, **8**, 2000153.
- 42 L. F. Abbott and W. G. Regehr, *Nature*, 2004, **431**, 796.
- 43 T. V. P. Bliss, G. L. Collingridge, R. G. M. Morris and K. G. Reymann, *Neuroforum*, 2018, **24**, A103.
- 44 E. R. Kandel, *Biosci. Rep.*, 2004, **24**, 475.
- 45 P. D. Roberts and C. C. Bell, *Biol. Cybern.*, 2002, **87**, 392.
- 46 R. S. Zucker and W. G. Regehr, *Annu. Rev. Physiol.*, 2002, **64**, 355.
- 47 A. Volianskis, G. France, M. S. Jensen, Z. A. Bortolotto, D. E. Jane and G. L. Collingridge, *Brain Res.*, 2015, **1621**, 5.
- 48 D. C. Rubin, A. E. Wenzel, J. Anderson, A. Boneau, J. Cerella, H. Crovitz, S. Hinton, A. Machado, B. Murdock, M. Serra, H.-O. Schiffman, J. Staddon, W. Wickelgren and J. Wixted, *Psychol. Rev.*, 1996, **103**, 734.
- 49 Y. Dan and M. Poo, *Neuron*, 2004, **44**, 23.
- 50 T. Celikel, V. A. Szostak and D. E. Feldman, *Nat. Neurosci.*, 2004, **7**, 534.
- 51 R. K. Mishra, S. Kim, S. J. Guzman and P. Jonas, *Nat. Commun.*, 2016, **7**, 11552.
- 52 H. Markram, W. Gerstner, P. J. Sjöström and T. Sakaba, *Front. Synaptic Neurosci.*, 2011, **3**, 4.
- 53 J. Meng, T. Wang, L. Chen, Q. Sun, H. Zhu, L. Ji, S. Ding, W. Bao, P. Zhou and D. W. Zhang, *Nano Energy*, 2021, **83**, 105815.

- 54 X. Zhang, R. Yu, X. Zhang, S. Wu, R. Yu, E. Li, D. Liu and C. Gao, *Matter*, 2022, **5**, 3023.
- 55 Y. Liu, D. Liu, C. Gao, X. Zhang, R. Yu, X. Wang, E. Li, Y. Hu, T. Guo and H. Chen, *Nat. Commun.*, 2022, **13**, 7917.
- 56 J. Meng, T. Wang, H. Zhu, L. Ji, W. Bao, P. Zhou, L. Chen and Q. Sun, *Nano Lett.*, 2022, **22**, 81.
- 57 R. Yu, L. He, C. Gao, X. Zhang, T. Guo, W. Li and H. Chen, *Nat. Commun.*, 2022, **13**, 7019.